Oxidation catalysis on Pt and Au : complexity of simple chemistry

Spronsen, M.A. van

Chapter 6

Effect of water on CO oxidation at low-coordination Au sites

6.1 Introduction

The recent history of Au catalysis started with the pioneering work of Haruta et al. [27]. In this and following studies, Au nanoparticles (NPs) were found to be active for CO oxidation, water-gas shift reaction, selective oxidation and hydrogenation/isomerization [147]. In the Netherlands, Au catalysis has successfully been studied amongst others in the group of Prof. B.E. Nieuwenhuys [233, 234].

In addition to being of fundamental, chemical interest, Au catalysis can hold the answer to some challenging problems in catalysis. One of these is the *low-temperature* and selective oxidation of CO. Traditionally used catalysts, such as Pt, only operate at high temperature. Au does not not have this requirement and has the potential to increase the efficiency of the automotive catalysts before the catalyst is at operating temperature. Additionally, Au can selectively oxidize adverse CO in hydrogen fuel cells.

Advances in our understanding of Au catalysis have recognized the importance of three factors: highly dispersed NPs, a reducible oxide support, and the presence of H_2O vapor to enhance the reactivity. These have inspired various explanations for the high reactivity of Au. Among these hypotheses are: the modified electron structures of small clusters [172], the presence of low-coordinated atoms [235], the existence of active sites on the NP-support perimeter, or spillover, i.e., diffusion from support to NPs of reaction intermediates.

Proving or disproving these theories on technical catalysts is very difficult. This is because precise characterization of the active sites both chemically and structurally is needed. This is where model catalysts come into play. They can represent one aspect of a real catalyst, while greatly reducing the inherent complexity of the technical catalyst.

Ideally, the full structural and chemical characterization is obtained under reaction conditions. Although recently developed surface science tools can give some of the desired structural [15, 19, 22] or chemical information [236], they have limitations. These tools are very challenging and usually operate at the signal-to-noise limit. As a consequence, these so-called in situ or operando techniques still depend on vacuum-based, surface science experiments to interpret the experimental results.

In this and our previous work, we undertook a surface science study using X-ray photoelectron spectroscopy (XPS) and temperature-programmed desorption (TPD) to answer elementary questions about the interaction of H_2O and Au, the oxidation of CO, and the role of low-coordinated atoms. In the previous chapter, we studied the interaction between H_2O and a stepped model catalyst, the Au(310) single-crystal surface. This surface is visualized in Figure 5.1. The surface consist of narrow (2–3 atom wide) terraces with a (100) structure separated by monoatomic (110) steps. The high step density provides many atoms with low coordination numbers, going as low as 6. The lowest coordinated atoms are found in the (110) step at the edge of the terrace. The high concentration of low-coordinated Au atoms makes it a good model for small NPs. However, because it is a single crystal the electronic structure remains that of metallic Au. Furthermore, the lack of an oxide support allows us to completely separate the effect of different aspects of the technical catalyst. The main results of the previous chapter are summarized as follows: low-coordinated atoms increase the H_2O-Au interaction, however, no H_2O dissociation was observed [161, 237].

As the high concentration of low-coordinated atoms is not enough to explain the promoting effect of H_2O, we focus on a different hypothesis to explain the role of H_2O. Water dissociation or H_2O-assisted activation of oxygen could occur on the support or on the NP-support perimeter. This can be followed by diffusion of the reaction intermediates to the facets of the NP, where they are able to react with CO. In our model catalyst, no oxide support was present. The reaction intermediates spilling over to the Au surface were produced in a different way. Adsorbed D_2O layers were exposed to low-energy electron irradiation to fragment D_2O. This treatment led to a mixtures of D_2O:O_{ad} on the surface, based on the XPS measurement. No significant amount of OD was detected. This mixture was tested for reactivity towards CO oxidation. The experiments were repeated at different temperatures to study the kinetic details of this reaction.

6.2 Experimental

The experimental details were thoroughly discussed in the previous chapter and only the most important aspects will be highlighted. All experiments were performed at the SuperESCA beamline, Elettra Sincrotrone Trieste, Italy. We used an ultra-high vacuum (UHV) system designed to study surfaces with high-resolution or time-resolved XPS. This system was equipped with a liquid-nitrogen cryostat, a quadrupole mass spectrometer (QMS), and equipment to measure low-energy electron diffraction (LEED).

A single crystal of Au, polished to the (310) plane[1] was cleaned with multiple cycles of Ar^+ sputtering[2] and annealing[3]. Surface crystallinity was checked with LEED and cleanliness was confirmed with XPS.

High-purity[4] D_2O and He were co-dosed after repetitive freeze-pump-thaw cycles to remove dissolved air. D_2O was used, because of the low background levels of both D_2O and D_2 in the residual gas of the vacuum chamber. Reproducible dosing was achieved by monitoring the O 1s signal from the surface while admitting D_2O/He to the vacuum chamber. After adsorption at a surface temperature of ∼100 K, the D_2O was exposed to electron irradiation for 5 to 720 s. These electrons were generated using the electron gun of the LEED system at an energy of 100 eV. For this purpose, the electron gun was completely defocused, with a resulting beam width of ∼5 mm and a sample current of 7–8 μA. The electron dose is reported in monolayer (with 1 ML equal to the number of Au atoms in the (310) surface: $1.14\times10^{19}m^{-2}$), based on the integrated sample current and the estimated beam size. The electron irradiation led to a sample temperature increase of 4–5 K.

XPS spectra were recorded at three different photon energies: 170 eV for Au $4f_{7/2}$, 650 eV for O 1s, and 400 eV for C 1s. Spectra were taken with normal emission and an incident angle of 70°. Furthermore, they were corrected by measuring the Fermi level. After this calibration, every spectrum was scaled by a constant factor, obtained by averaging the background over a 0.5 eV interval on the low binding energy side,

[1] accuracy of 2.3°
[2] energy of 1 keV, for a few minutes
[3] in UHV, 860 K
[4] D_2O, 99.95 at.% D, Aldrich; He, 6.6 N purity

to correct for changes in beam intensity. After scaling, a linear fit to the background was subtracted. Fitting of the resulting spectra was achieved using a Doniach-Šunjić function [94] convoluted with a Gaussian line shape. The D_2O coverage was estimated by comparing the O 1s integral with that of a saturated CO overlayer at 105 K, which equals a coverage of 50 % of the step atoms or 0.167 ML [161, 208]. These integrals were measured at 1205 eV to decrease the effect of energy-dependent fluctuations of the photoemission cross section, caused by photoelecton diffraction. These are stronger, closer to the absorption edge. This calibration of the coverage was confirmed by analyzing the relative intensities of the O 1s and Au $4f_{7/2}$ peaks, see previous chapter.

During the experiments, some increase in C was detected (see SI). It was identified as CO, and possibly some amorphous or graphitic C, and possibly carbidic AuC_x. This C buildup was unavoidable due to the lengthy nature of these experiments, typically several tens of minutes. These species were unrelated with X-ray beam exposure and only showed a slow increase over time and for CO, a decrease with electron irradiation. The total amount was rather low, typically 2–3 % with a maximum of 4.7 %, which mainly consisted of CO. The coverage estimation was based on the coverage of the saturated CO overlayer (105 K, 400 eV) [161, 208]. Furthermore, we believe that they were spectator species, since our results showed no correlation with their coverage.

6.3 Results

6.3.1 Formation of reaction intermediates

H_2O does not adsorb dissociatively on Au(310) under UHV conditions and, hence, the coadsorption of H_2O and CO did not lead to CO oxidation [161, 237]. To study reaction of water with CO on this Au model catalyst without oxide support, we activated D_2O by electron irradiation.

Figure 6.1 shows the XPS O 1s spectra after increasing amounts of 100 eV electron irradiation. The figure shows the result of an experiment in which the surface was stepwise irradiated. The experiment started after dosing D_2O up to a coverage of 0.5 ML, referred to as pristine D_2O. The electron irradiation induced a strong intensity decrease of the major peak. Furthermore, the peak shifted to lower binding energies (532.3 to 531.4 eV) with increasing electron dose. In addition, the peak around 530 eV grew significantly compared to the pristine D_2O layer and the peak shifted from 529.9 to 529.7 eV.

A quantitative view of the effect of electron irradiation was obtained by fitting the O 1s spectra with four peaks. Two were used to account for adsorption of pristine D_2O (black, 532.8 eV and red, 532.2 eV). The origin of these molecular peaks is discussed in the previous chapter. In short, the peak at 532.8 eV was assigned to both multilayer D_2O and D_2O bonded to ninefold-coordinated Au atoms. The other peak, at 532.2 eV was attributed to D_2O bonded to sixfold- and eightfold-coordinated Au atoms. To account for the changes induced by the electron irradiation, one new peak (blue, ∼531.6 eV) and one peak for O_{ad} (green) were needed. To obtain the best fit, the binding energy for the former shifted from 531.9 to 530.9 eV, with an average of 531.6 eV. The appearance of the new species on the surface indicated the

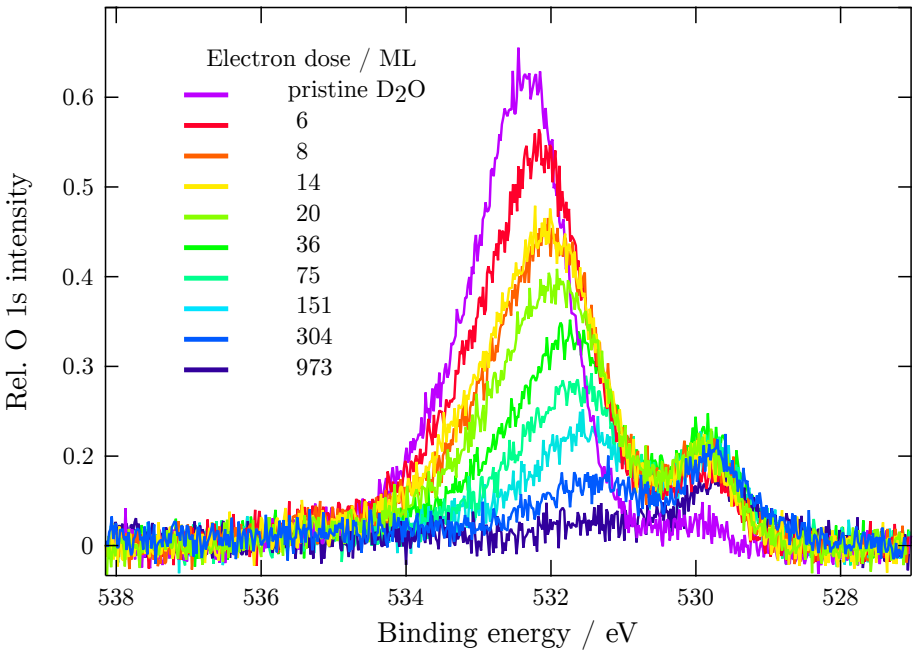

Figure 6.1: XPS O 1s spectra showing the effect of increasing electron irradiation dose on the adsorbed D_2O layer. Several changes are notable: an intensity decrease of the main peak, a shift to lower binding energies, and the growth of the peak around 530 eV. Spectra were recorded at ∼100 K.

formation of hydroxides or the O_{ad}-stabilisation of D_2O. The actual assignment will be given in the discussion section.

Three fitted spectra are presented in Figure 6.2. Figure 6.2a depicts a spectrum prior to electron irradiation, showing intact D_2O, fitted with two separate peaks. After a small amount of electron irradiation (36 ML, Figure 6.2b), the feature corresponding to O_{ad} developed into a significant contribution to the spectrum and a peak at ∼531.6 eV appeared, while the peaks assigned to intact D_2O strongly decayed. The total O 1s intensity decreased considerably from 0.5 to 0.3 ML, which we attributed to electron-stimulated desorption. Thermal desorption could be excluded, since the temperature increase during electron irradiation was too small. This was confirmed by TPD experiments that showed no desorption of H_2O at 100±10 K (see previous chapter and References 161 and 237). With increasing irradiation dose (304 ML), the total O coverage decreased to 0.05 ML. The surface was covered by roughly equal amounts of O_{ad} and the unknown species, which was reduced by a factor 3.

The fitted peaks were integrated, normalized to obtain the O coverages and plotted as a function of the electron dose as shown in Figure 6.3. The figure shows a strong exponential decay in the D_2O coverage upon electron irradiation. At the same time,

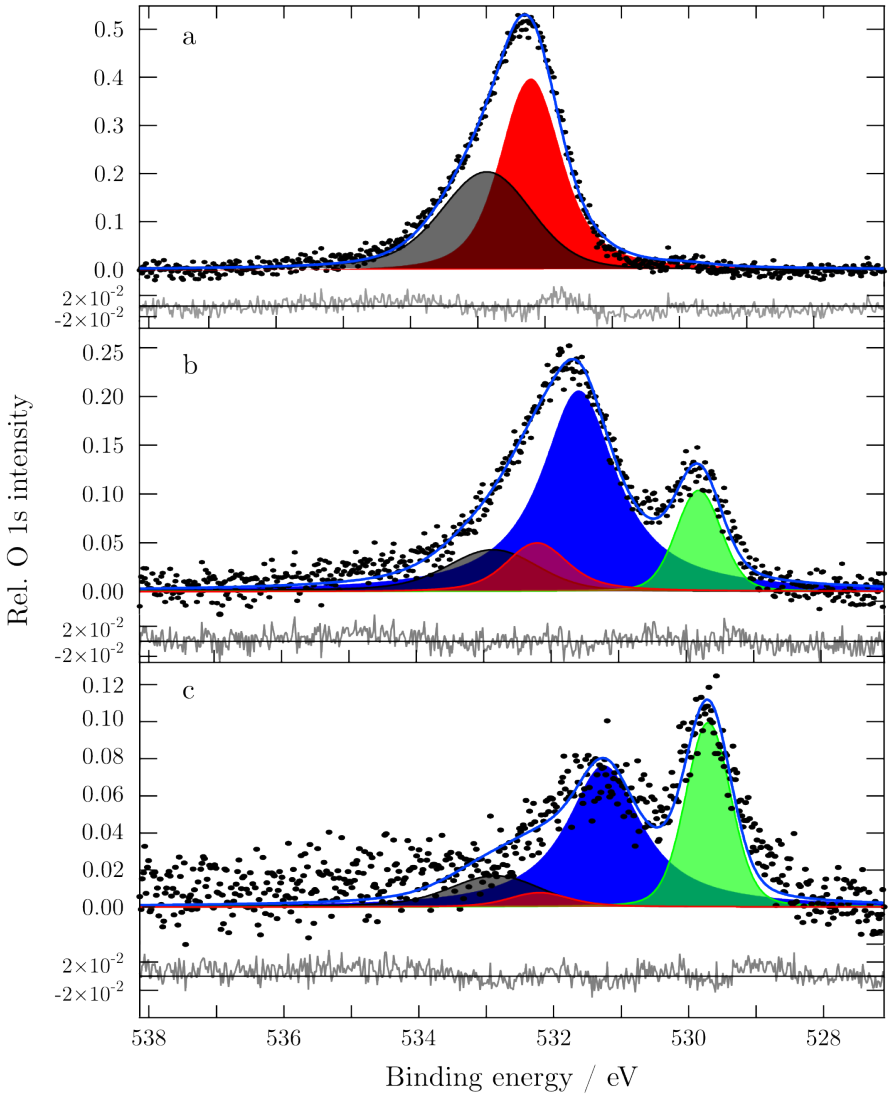

Figure 6.2: Fits of several O 1s spectra to show the model to describe the effects of the electron irradiation. Peaks represent: D_2O, weakly bonded (black) and Au bonded (red), peak at ∼531.6 eV (blue), and O_{ad} (green). (a), no electron irradiation. (b), 36 ML electron dose. (c), 304 ML electron dose. Lower panels of figures give the residual spectra. Spectra were recorded at ∼100 K.

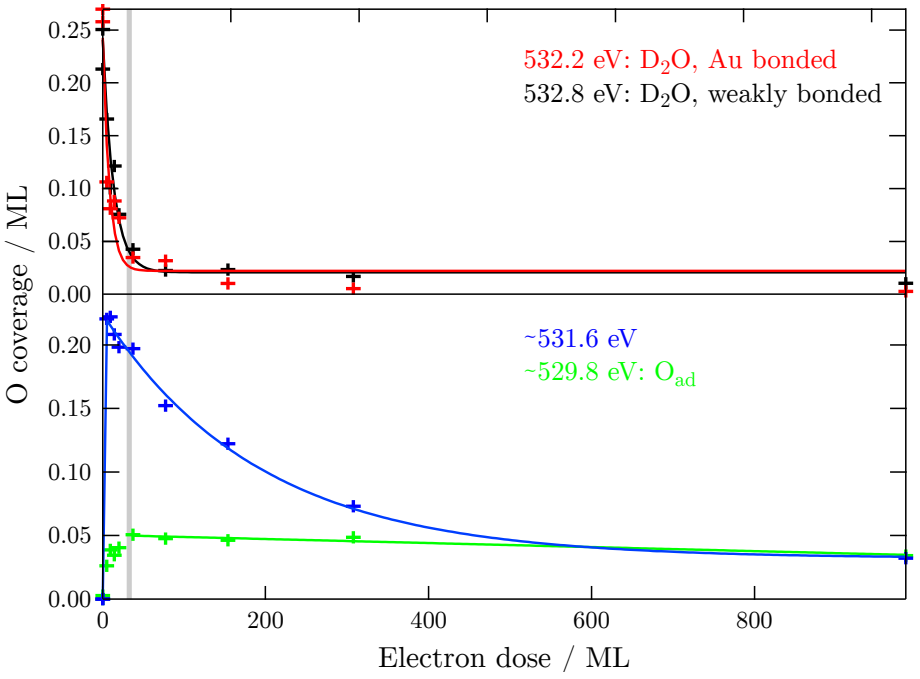

Figure 6.3: Coverage of different O-containing species plotted versus electron irradiation dose. Strong decrease of D_2O (red and black) caused by desorption and fragmentation was observed for a small electron dose. In parallel, the peak at ~531.6 eV increased, reaching a maximum after an electron dose of 36 ML, after which it decreased again. The O_{ad} peak showed similar behavior, but saturated at 0.05 ML. The grey bar indicate the XPS fits obtained after an electron dose of 36 ML (Figure 6.2b).

the intensity of the peak at ~531.6 eV was rapidly increasing for an electron dose up to 36 ML, after which it showed a modest decrease. The O_{ad} peak increased initially, after which it saturated around 0.05 ML, followed by a slow, gradual decrease. The relative intensity of the peak at ~531.6 eV rapidly increased to 8 times that of the O_{ad} peak within the first 8 ML of electron irradiation. After this initial increase ($\gtrsim$30 ML), the relatively intensity started to decrease.

Figure 6.4 shows four Au $4f_{7/2}$ spectra. None of the spectra showed any sign of Au oxides. These oxides would be expected around 85.2–86.0 eV [238–251] (indicated by the yellow region in Figure 6.4) The largest difference can be observed between the spectrum of the clean Au(310) surface and that obtained with 0.5 ML D_2O adsorbed. Electron irradiation induced only small changes in the spectra. The total intensity increased with increasing electron dose, due to desorption of D_2O. Other changes were an increase in the shoulder around 84.6 eV and the decrease in the shoulder at 83.7 eV. All changes were very modest and the latter two changes were reversed by larger doses of electron irradiation.

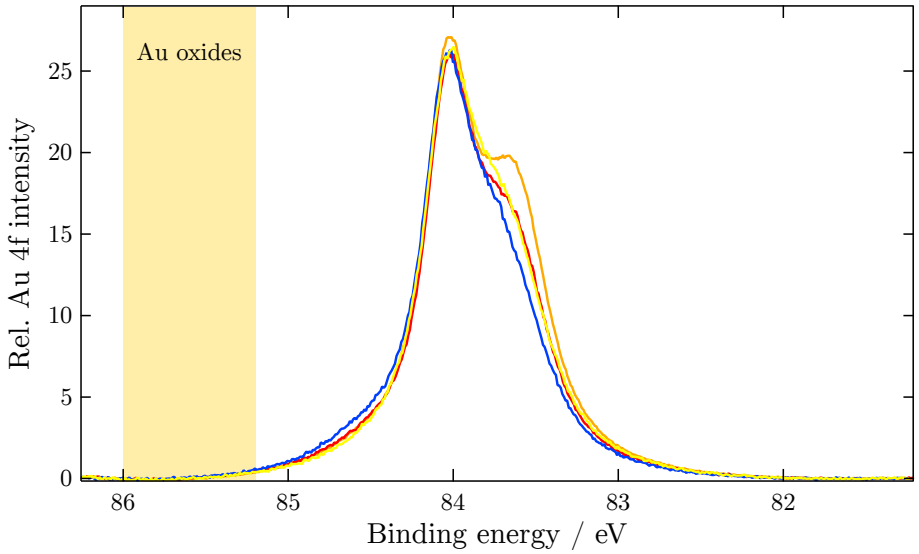

Figure 6.4: Au $4f_{7/2}$ spectra obtained during various stages of the experiment: clean Au(310) surface (orange), after adsorption of 0.5 ML D_2O prior to electron irradiation (red), after an electron dose of 8 ML (blue), and after an electron dose of 973 ML (yellow). Possible Au oxides would be expected in the yellow region between 85.2–86.0 eV.

6.3.2 CO oxidation by activated D_2O

For the next set of experiments, a reproducible amount of D_2O (0.5±0.1 ML) was adsorbed while monitoring the O 1s signal. After adsorption, the surface was irradiated with a fixed electron dose (36 ML) to obtain a mixture close to that indicated by the grey bar in Figure 6.3. This resulted in a mixture of D_2O, O_{ad}, and possibly hydroxide or O_{ad}-stabilized D_2O. The total coverage of this mixture was ∼0.3 ML. In this mixture, the O_{ad} content was 21±1 %. The followed procedure resulted in mixtures with very reproducible composition, with only modest variation in absolute coverage. The prepared mixture was exposed to CO, at the highest attainable pressure ($\sim 1\times10^{-7}$ mbar) that allowed us to measure the O 1s spectra simultaneously. This corresponded to a CO flux of 0.03 ML/s.

Even at temperatures as low as 105 K, we observed reactivity. Figure 6.5 presents the areas of the fitted peak as a function of time, measured while exposing the surface to CO. Two distinct cases are shown here: one (Figure 6.5a) of a reaction at 137 K, which is below the onset of H_2O desorption. The other (Figure 6.5b) shows a dataset recorded at 153 K, i.e., at the onset of H_2O desorption (see previous chapter and References 161 and 237). Both situations clearly showed a strong decrease in O_{ad} and in the ∼531.6 eV peak and were directly correlated with the CO exposure.

In both measurements, the photoemission spectra show an increase in the peaks associated with pristine D_2O. In the lower temperature experiment (Figure 6.5a), this

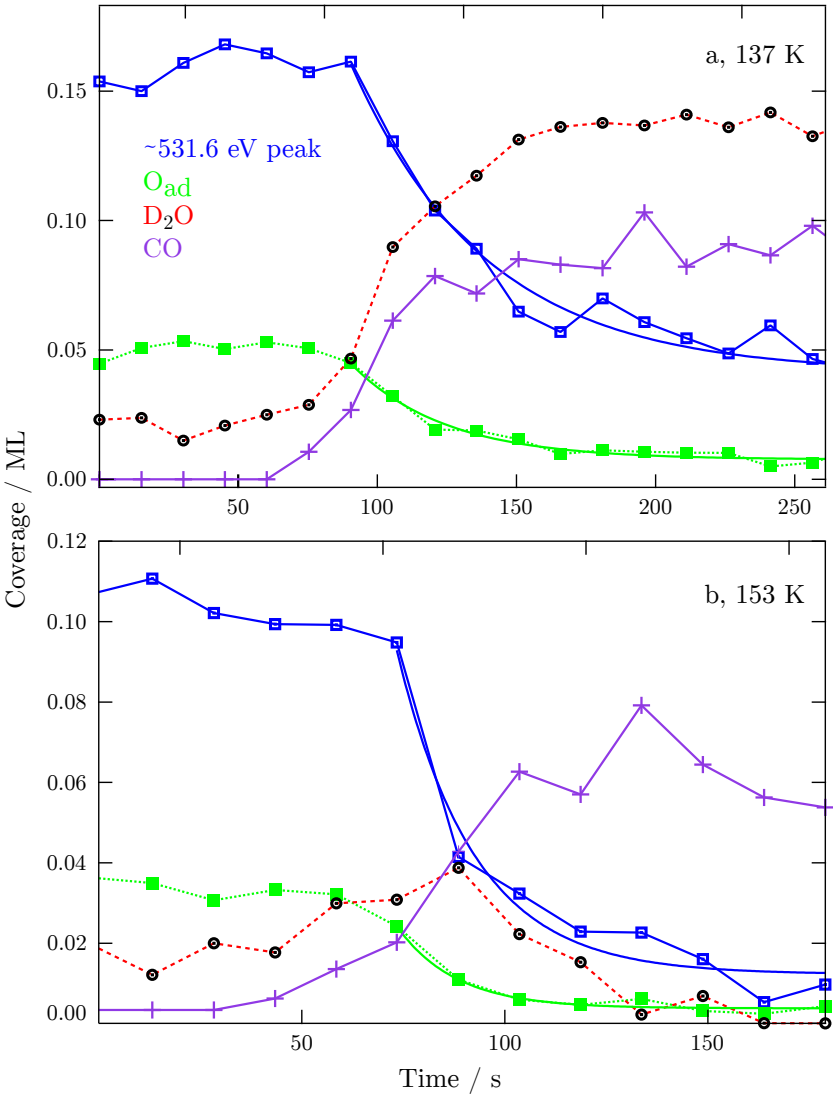

Figure 6.5: Reaction of the fragmented D_2O mixture with CO at two different temperatures one below the H_2O desorption temperature, 137 K (a) and one at the desorption temperature, 153 K (b), lines depict the peak areas for the combined D_2O peaks of 532.2 and 532.8 eV (dashed, red line with black circles), the peak at ~531.6 eV (blue, solid line with open squares), O_{ad} (dotted, green line with solid squares), and CO (purple line with crosses). Note the shorter time scale on the axis of (b).

is most prominent, since the surface temperature was not high enough to facilitate desorption. At 153 K, D_2O can desorb and only a transient peak in D_2O coverage was observed, which quickly decayed. Interestingly, D_2O showed a higher thermal stability before the reaction as it remained adsorbed on the surface. This D_2O was indistinguishable with XPS from pristine D_2O adsorbed on Au(310).

Activation energies

To determine the apparent activation energies, CO oxidation experiments were performed under a constant p_{CO} of $(8\pm1.8)\times10^{-8}$ mbar. The experiments were repeated for three temperatures: 125 ± 2, 137 ± 0, and 153 ± 2 K. The decrease in O_{ad} and in the ~531.6 eV peak was fitted with an exponential decay:

$$\theta(t) = \theta_i \exp(-t/\tau)$$

in which $\tau = k_d/(k_r S_{CO} F_{CO})$ (see SI) with k_d and k_r as the rate constants for CO desorption and the reaction with CO, S_{CO} as the CO sticking coefficient and F_{CO} as the CO flux impinging on the surface. A plot of $\ln(1/\tau)\times R$ versus $\frac{1}{T}$ yields a line with the slope: $-E_{a,app} = -E_{a,r} + E_{ad,CO}$. In this formula, $E_{a,app}$ is the apparent activation energy, $E_{a,r}$ the activation energy of the CO oxidation reaction, and $E_{ad,CO}$ the adsorption energy of CO. Figure 6.6 gives this plot and it shows that for both the decrease in O_{ad} and the decrease in the ~531.6 eV peak a similar slope was obtained. The resulting apparent activation energies were 5 ± 2 and 7 ± 2 kJ/mol, respectively.

The linear fits yielding the apparent activation energies were constructed using the orthogonal distance regression (ODR) algorithm[5]. The ODR fit took uncertainties in both temperature and τ into account.

From the apparent activation energies, the activation energy for the Langmuir-Hinshelwood reaction with CO can be derived by adding the CO adsorption energies [161]. These were reported to be 21 ± 3 and 37 ± 5 kJ/mol, depending on the nearest-neighbor distance of the CO molecules, which were adsorbed on the Au step edges. This resulted in activation energies for the reaction of O_{ad} with CO of 26 ± 4 and 42 ± 5 kJ/mol or 0.27 and 0.44 eV, depending on the CO adsorption site. These barriers agreed well with the barriers found for CO oxidation with O_{ad} on Au(211) [252] and is between the barriers for Au(111) [221] and Au(110) [253, 254] (see Table 6.1).

During the CO exposure, both the peak ascribed to O_{ad} and the peak at ~531.6 eV were exponentially decaying to an asymptotic value that was above zero. In other words, a certain amount of both species remained on the surface and was unreactive towards CO. This unreactive fraction increased with decreasing temperature. This can be observed when the exponential decays of Figure 6.5a are compared with those of Figure 6.5b. For example, the unreactive O_{ad} fraction increased from 25 % of the initial O_{ad} coverage at 137 K to 36 % at 125 K.

[5]Igor Pro 6.05 with ODRPACK95

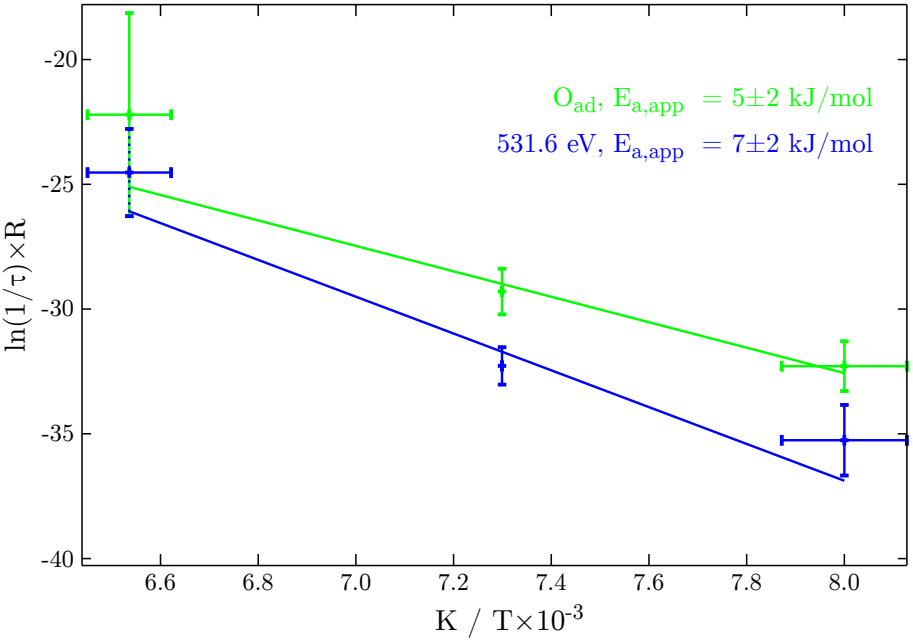

Figure 6.6: plot of $\ln(1/\tau)\times R$ versus 1/T for both the decrease in O_{ad} and the ~531.6 eV peak. The apparent barriers were derived from the slope of the fitted line, which resulted in 5 ± 2 and 7 ± 2 kJ/mol for O_{ad} and the ~531.6 eV peak, respectively. Reactions were all performed with a p_{CO} of $(8\pm1.8)\times10^{-8}$ mbar.

Surface	T range	$E_{a,app}$	$E_{a,r}$	Reference
Au(111)	250–375	–10±3	10±3	221
Au(110)	275–440	8±2	<42	253
	200–400	–1.8±0.9	57	254
Au(211)	200–400	-7	20 & 43	252
Au(310)	125–153	(5–7)±2	(26–28)±4 &	This work
			(42–44)±5	This work

Table 6.1: CO oxidation apparent and reaction activation energies in kJ/mol for single-crystal surfaces. Also, the temperature ranges in K are given over which the activation energies were determined.

6.4 Discussion

The effect of electron irradiation on the D_2O layer can be explained in three steps. The most discernible process occurring during irradiation was electron-stimulated desorption of water, which caused the decrease in intensity of the largest peak at 532.3 eV. Second, some D_2O dissociated upon irradiation and formed O_{ad} on the surface. The formation of O_{ad} was observed by the intensity gain of the peak at 529.9–529.7 eV, which we previously assigned to O_{ad} [237]. Because the reported binding energies in the literature

of O_{ad} show significant variation and also overlap with the binding energies of Au oxides, we base this assignment on the absence of any Au oxide peaks in the Au $4f_{7/2}$ spectra. Third, the shift of the main XPS peak from 532.3 to 531.4 eV, is interpreted as the appearance and growth of a new XPS peak at lower binding energies as compared to the pristine D_2O peaks. It could stem from the formation of hydroxides on the surface.

The possible formation of hydroxides on Au surfaces from coadsorbed D_2O and O_{ad} via

$$D_2O + O_{ad} \rightarrow 2\ OD \tag{6.1}$$

has been debated in literature. Several studies indicate that at least very small amounts of hydroxides form on Au(111). This was based on the observed isotope exchange between isotopically labeled H_2O and coadsorbed O_{ad} [255] as was the case for Au(110) [153]. In similar experiments, it was found that these hydroxides are reactive towards CO [256, 257] on Au(111). However, the hydroxide signature was not detected on the same surface with infrared spectroscopy [255], which had a detection limit of ∼0.05 ML. On the stepped Au(997) surface, the ultraviolet photoelectron spectrum showed a peak accredited to hydroxide [223].

DFT calculations show that the formation of hydroxides on Au(111) from coadsorbed H_2O and O_{ad} is endothermic (0.03–0.21 eV) [257–259], with relatively small barriers of 0.11–0.33 eV [257, 259]. If we make the simplification that the DFT-calculated energies are equal to the free energies, this would lead to equilibrium constants of $0.03–3\times10^{-11}$ at 100 K and $0.11–2\times10^{-7}$ at 160 K. This supports the view that if hydroxides are formed on the Au(111) surface, their concentration is small, most likely lower than the detection limit of regular surface science techniques. On Au(110), however, the formation of hydoxides is greatly exothermic [258], indicating that this reaction is strongly structure sensitive. Also on other stepped surfaces, e.g., Pt, the formation of O_{ad} versus OH has been shown to depend on the precise structure of the step [260].

Alternatively, it could originate from D_2O stabilized by H bonding to nearby O_{ad}. Three arguments favor the assignment of the ∼531.6 eV peak to O_{ad}-stabilized D_2O through H bonding and not to the formation of OD. First, the observed stoichiometry as deduced from the increase in D_2O upon CO oxidation is incompatible with reaction of CO with OD. The ratio of D_2O increase to decrease in area of the ∼531.6 eV peak was 1.20 at 125 K and 0.76 at 137 K. This is significantly higher than 0.5, which would be expected if the peak was originating from hydroxide. In that case, the hydroxide would have either reacted via

$$OD + CO \rightarrow COOD \tag{6.2}$$

$$COOD + OD \rightarrow CO_2 + D_2O \tag{6.3}$$

or

$$2\ OD \rightarrow D_2O + O \tag{6.4}$$

$$CO + O \rightarrow CO_2 \tag{6.5}$$

In both cases, half of the hydroxide groups would react (directly or indirectly) with CO, while the other half would form D_2O. Because the experimentally derived ratio was larger than 0.5, we propose:

$$O\text{–}D_2O + CO \rightarrow CO_2 + D_2O \tag{6.6}$$

The expected ratio for this reaction would be 1 or higher, depending on the number of D_2O molecules that are interacting with every O_{ad}. The value found at 125 K was slightly higher than 1, but within the estimated uncertainty of the fits. At higher temperature, this ratio decreased, which can be explained by desorption of some D_2O during the reaction. At 153 K, only a modest transient increase in D_2O was observed.

Our second argument to ascribe the peak at ∼531.6 eV to O_{ad}-stabilized D_2O relies on the activation energies found for reaction with CO. If the unknown species indeed was O_{ad}-stabilized D_2O, and not OD, similar values were to be expected because the decrease in both species is caused by a single reaction (reaction 6.6). In the case of parallel reactions of CO with O_{ad} and OD, it would be coincidental that both CO oxidation with O_{ad} and OD would have similar barriers.

Finally, the position of this peak around 531.6 eV suggested that it is not a hydroxide species. The shift of the peak with respect to that of pristine D_2O was around 1 eV, equal to the 1.0 eV shift reported for Au(111), explained by stabilization of H_2O by H bonding to O_{ad} [221]. In a similar experiment on the same surface, a 2.0 eV shift from the binding energy of H_2O was detected upon H_2O and O_{ad} coadsorption, which was tentatively assigned to OH formation [231]. On the Au(997) surface, a shift of 0.7 eV was found between the peaks assigned to H_2O and H_2O affected by O_{ad}, respectively [223]. We note that our spectra show a hint of a peak on the edge of the XPS detection limit at 530.9 eV, which is close to the binding energy (530.7 eV) of the peaks attributed to hydroxides on Au(111) [231] and on Au(997) [223]. The intensity of this species is, however, almost insignificant compared to that of D_2O and O_{ad}.

With three arguments to assign the peak at ∼531.6 eV to D_2O H bonded to O_{ad} and no arguments to assign it to OD, we continue with a comparison of the peak areas of O_{ad} and of O_{ad}-stabilized D_2O (Figure 6.3). Interestingly, this comparison reveals that up to 6–8 D_2O molecules were stabilized by a single O_{ad} atom. The interaction of O_{ad} with several D_2O molecules makes it very plausible that the adsorbates did not segregate into islands, but were completely mixed.

The D_2O:O_{ad} mixture on the Au(310) was highly reactive towards CO, even at temperatures as low as 105 K. However, the comparison of the activation energies of this surface with the Au(111) surface shows that the presence of steps does not increase Au's reactivity, contrary to what is often believed to be the effect of surface corrugation. This can be explained by the fact that steps stabilize the reactants more than the transition state of the CO oxidation reaction. On a real supported catalyst, the turnover is not solely determined by the activation energies of reactions 6.5 and 6.6. It also depends on the coverage of the oxidant. This could be greatly affected by the low-coordinated Au atoms, which are likely to bind O_{ad} stronger in the vicinity of the steps, perhaps even stabilizing the particle's shape. The net result could be a more active catalyst.

Our experiments give evidence that OD is not stable with respect to D_2O and

O_{ad}. Therefore, O_{ad} is the major oxidant in CO oxidation. Hydroxide could still be important as a possible spillover product, which would probably be more mobile than O_{ad} on the Au surface. This hydroxide species will form O_{ad} and D_2O near the active site of the Au NP, after which O_{ad} reacts with CO to form CO_2.

At lower temperature, less D_2O desorbed in our reactivity measurements and as a result an increasing fraction of O_{ad} remained on the surface. This O_{ad} was completely unavailable for the reaction with CO. Possibly, it was strongly bonded into a H-bond network formed by the D_2O. Therefore, the reported, promotional role of water [28] should be fulfilled on the supporting oxide and not on the Au NP itself. On the surface of the Au NP, too much water has a poisoning effect on CO oxidation.

6.5 Conclusions

We have shown that a mixture of O_{ad} and D_2O can be created by electron irradiation of a molecular adsorbed D_2O layer without producing Au oxides. This is a major advantage over studies relying on decomposition of O_3 to produce active species, as such harsh oxidation may lead to formation of Au oxides. Those do not represent the actual catalyst well. Also, in our mixture of O_{ad} and D_2O with low-coordinated Au atoms, hydroxides are not significantly present. Similar to extended (111) terraces, they seem to highly favour dehydrogenation of hydroxides to O_{ad}. Hence, we only observe reaction from atomic O_{ad} with CO. As H_2O was previously shown not to dissociate on Au, we conclude that the role of water in promoting CO oxidation can lie in the supply of O-containing species by the catalyst's support. Probably in the form of OH, they can spill over to Au NPs, where dehydrogenation to O_{ad} is highly favoured. We have shown here through a kinetic analysis that reaction of O_{ad} with CO is not significantly affected by the stronger binding to low-coordinated Au sites in comparison to terrace-bound O_{ad}. Finally, we note that excess water may have a poisoning effect on CO oxidation by overcrowding O_{ad}, making it inaccessible for reaction with CO.

Supplementary information – Effect of water on CO oxidation at low-coordination Au sites

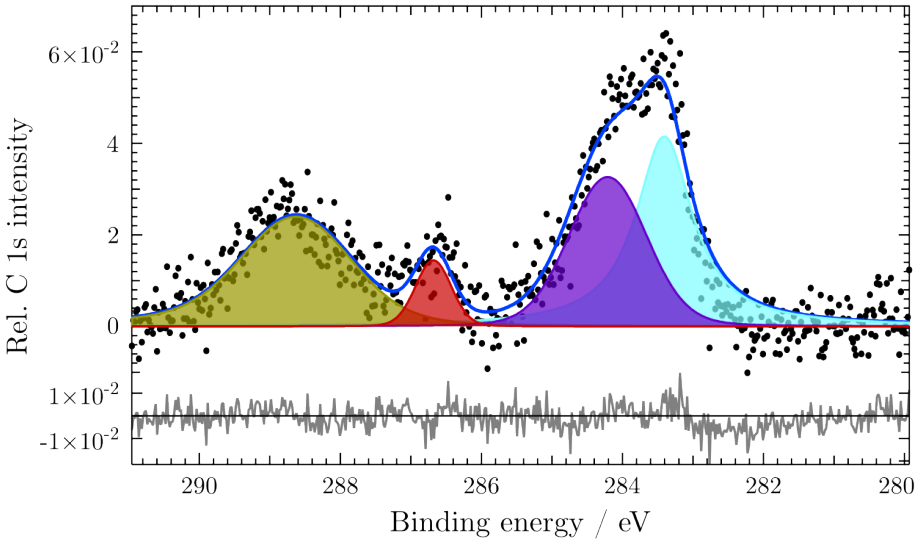

Figure 6.7: One example of a C 1s spectrum measured at 109 K after an electron irradiation dose of 20 ML on 0.5 ML D_2O/Au(310). Four distinct peaks were observed and were assigned as follows: CO (yellow/brown, 288.6 eV) [208], graphitic or amorphous C (purple, 284.2 eV), and carbidic AuC_x (light blue, 283.4 eV). The origin of the small peak (red/brown) at 286.7 eV remains unknown. Lower panel of the figure gives the residual spectrum.

Introduction

This chapter provides supporting information to the previous chapter. It includes a set of C 1s spectra and a derivation for the kinetic model. The set of spectra was recorded during the experiments in which a fixed amount of D_2O was irradiated stepwise with 100 eV electrons. All spectra were analyzed as described in the previous chapter.

Electron irradiation, C 1s spectra

A small increase in C was noticed during the electron-irradiation experiments. One example of a typical C 1s spectrum is depicted in Figure 6.7. It shows that 4 different carbon species were present. Based on their binding energies, we identified CO (yellow/brown, 288.6 eV) [208] and speculate that graphitic or amorphous C (purple, 284.2 eV) [261], and carbidic AuC_x (light blue, 283.4 eV) [101] were present. The small peak (red/brown) at 286.7 eV remained unidentified.

The C 1s spectrum of the Au(310) surface saturated with CO at 105 K is illustrated in Figure 6.8. CO binds to half of the step atoms, corresponding to a coverage of 0.167 ML [161, 208]. The integral of this spectrum was used to quantify the C contamination.

To learn more about the origin of these peaks, the fitted peaks were integrated

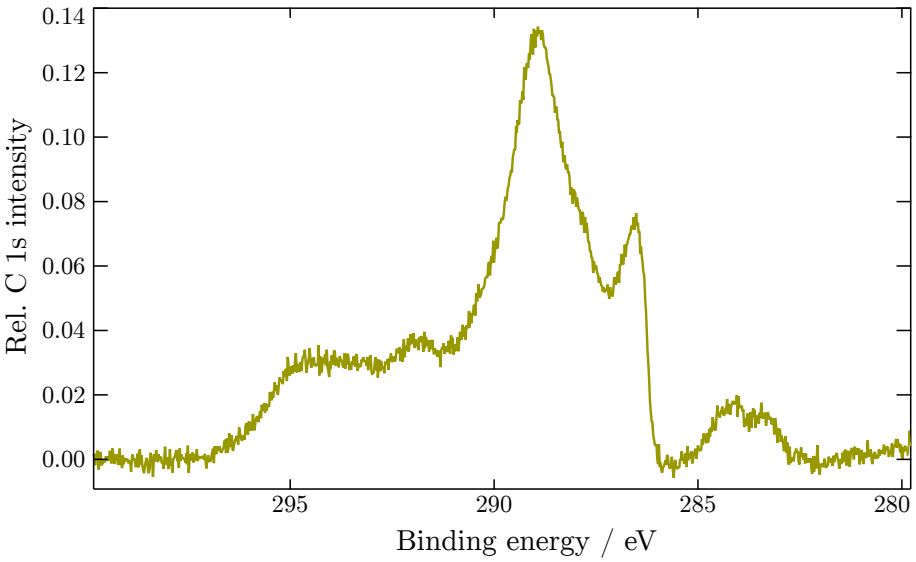

Figure 6.8: C 1s spectrum from a saturated CO layer at 105 K, which corresponds to a coverage of half of the step atoms (0.167 ML) [161, 208].

and plotted versus all experimental parameters to search for a correlation. These parameters included: electron-irradiation dose, time in experiment, number of total XPS scans performed, and number of O 1s, C 1s, and Au $4f_{7/2}$ spectra recorded. The results are plotted in Figure 6.9. The peak assigned to CO was largest directly after dosing D_2O and decreased with increasing amount of electron irradiation, due to electron-stimulated desorption. The peaks assigned to graphitic or amorphous C and carbidic AuC_x showed a linear increase over time. The coverage of graphitic or amorphous C increased linearly with time, but decreased after higher doses of electron irradiation. In this regime, an interplay between adsorption and electron-stimulated desorption could have determined the coverage. The carbidic AuC_x showed no dependence on X-ray or electron exposure and, therefore, we do not believe that it was caused by fragmentation of other C species. Instead, it is possible that C segregated from the bulk of the Au single crystal. The unknown peak at 286.7 eV did not show any correlation and had a constant intensity during the experiment. The typical amount of C contamination was 2–3 %, with a maximum of 4.7 %.

Kinetic model

The kinetic model used to obtain the CO oxidation reaction barrier was previously explained in detail in References 253 and 254. Therefore, only a brief derivation will be given here.

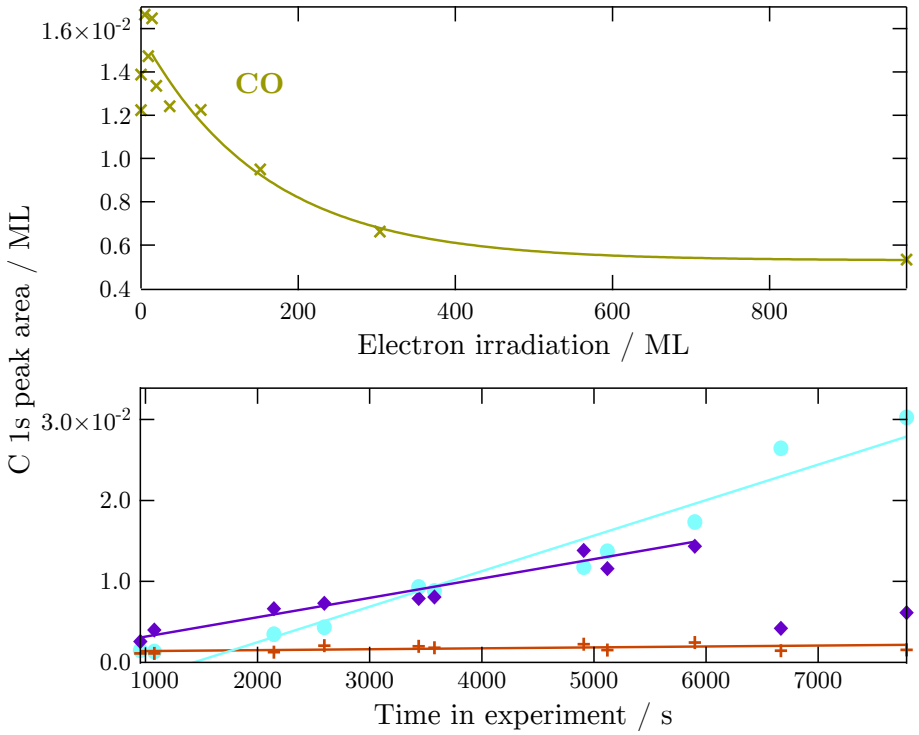

Figure 6.9: Areas of fitted C 1s peaks plotted versus the amount of electron irradiation for CO and versus the experimental time for the other peaks. The CO peak showed an exponential decrease with increasing electron-irradiation dose. The intensities of the graphitic or amorphous C (purple) and the carbidic AuC_x (light blue) peaks were linearly increasing over time. The unknown peak (red) at 286.7 eV had a constant intensity during the experiment.

If we assume a Langmuir-Hinshelwoood reaction between CO and O_{ad}, which react according

$$CO + O_{ad} \rightarrow CO_2 \tag{6.7}$$

then the rate of CO_2 formation can be expressed as

$$R_{CO_2} = -\frac{d\theta_O}{dt} = k_r \theta_O \theta_{CO} \tag{6.8}$$

in which θ represents the coverage of O_{ad} and CO, respectively, and k_r the rate constant for this reaction. For the CO coverage, we can assume steady-state conditions, i.e.,

$$\frac{d\theta_{CO}}{dt} = 0 = S_{CO} F_{CO} (1 - \theta_{CO}) - \theta_{CO} (k_d + \theta_O k_r) \tag{6.9}$$

In this formula, S_{CO} is the CO sticking coefficient and F_{CO} the CO flux impinging on the surface. Furthermore, the simplification was made that the CO coverage was

not influenced by the coverage of other adsorbates. For the reactivity experiments, a low flux of roughly 0.03 ML/s was used. In this case, we approximate that $1-\theta_{CO} \approx 1$, which leads to

$$\theta_{CO} = \frac{S_{CO} F_{CO}}{k_d + \theta_O k_r} \tag{6.10}$$

and

$$-\frac{d\theta_O}{dt} = \frac{k_r \theta_O S_{CO} F_{CO}}{k_d + \theta_O k_r} \tag{6.11}$$

Equation 6.11 leads upon integration to:

$$\ln\left(\frac{\theta_O}{\theta_{O,i}}\right) + \frac{k_r}{k_d}(\theta_O - \theta_{O,i}) = -\frac{k_r S_{CO} F_{CO}}{k_d} t \tag{6.12}$$

In this formula $\theta_{O,i}$ is the initial O_{ad} coverage. At least for the initial reaction, when $\theta_O - \theta_{O,i}$ is small, this can be approximated with

$$\ln\left(\frac{\theta_O}{\theta_{O,i}}\right) = -\frac{k_r S_{CO} F_{CO}}{k_d} t \tag{6.13}$$

which can be rearranged into

$$\theta_O(t) = \theta_{O,i} \exp(-t/\tau)$$

in which $\tau = k_d/(k_r S_{CO} F_{CO})$. The slope of $\ln(1/\tau) \times R$ plotted versus $1/T$ results in the apparent activation energy

$$-E_{a,app} = -E_{a,r} + E_{ad,CO} \tag{6.14}$$

from which the activation energy for CO oxidation, $E_{a,r}$ can be determined when the CO adsorption energy, $E_{ad,CO}$, is known.